Submitted to Journal of the Electrochemical Society as an article.
Scanning Ion Conductance Microscopy of Nafion-modified Nanopores
Kristen Alanis, ^a Zuzanna S. Siwy, ^b Lane A. Baker* ^a
^a Department of Chemistry, Texas A&M University, College Station, TX 77843
^b Department of Physics and Astronomy, University of California, Irvine, CA 92697
*Corresponding Author: lane.baker@chem.tamu.edu lane.baker@tamu.edu

Abstract

Single nanopores in silicon nitride membranes are asymmetrically modified with Nafion and investigated with scanning ion conductance microscopy, where Nafion alters local ion concentrations at the nanopore. Effects of applied transmembrane potentials on local ion concentrations are examined, with the Nafion film providing a reservoir of cations in close proximity to the nanopore. Fluidic diodes based on ion concentration polarization are observed in the current-voltage response of the nanopore and in approach curves of SICM nanopipettes in the vicinity of the nanopore. Experimental results are supported with finite element method simulations that detail ion depletion and enrichment of the nanopore/Nafion/nanopipette environment.

Introduction

lon transport is a crucial aspect of any electrochemical process, and plays significant roles in technological applications such as desalination, electrophoresis, and redox flow batteries. Interfacial chemistry has proven an important route to enhancing selectivity and control in ion transport. Advances in micro/nanoscale fabrication, small scale fluidic have led to concomitant advances in fundamentals and applications of nanofluidic platforms in sensing and separation applications. 1-7 At small spatial scales, unique transport regimes are encountered that provide opportunities to tune nanoscale ion transport. For instance, enrichment and separation of ions has been achieved in microfluidic systems by exploiting ion concentration polarization (ICP).8-11 ICP is an electrokinetic phenomenon that typically occurs due to changes in transport of charged ions (i.e. cations or anions), for example at a nanochannel-microchannel junction or due to the presence of an ionpermselective membrane. In these examples, the surface charge of the nanochannels or the intrinsic charge of the ion-exchange membrane dictates the charge carrier in the system, and in turn, selectivity in ion transport. Mobile counterions preferentially transported across the nanochannel/membrane lead to simultaneous ion depletion on one side and ion enrichment on the opposite side. Formation of ion enrichment and depletion zones can be inferred from current-voltage characteristics^{12, 13} and have been spatially resolved in real-time by fluorescence measurements. 14-16

In this report, we have applied scanning ion conductance microscopy (SICM)¹⁷ to elucidate local ion concentration spatially in the enrichment and depletion zones induced by transmembrane potentials across Nafion-modified silicon nitride nanopores. We have previously demonstrated the ability to probe localized ion concentrations such as the

electrical double layer of charged surfaces with SICM by monitoring the ion current through the nanopipette at different probe to sample distances. 18-20 Nafion is a prominent cation exchange membrane with wide utility in diverse technologies. Composed of a polytetrafluoroethylene (PTFE) backbone with side chains that have terminal sulfonate groups (SO₃-), the hydrated morphology of Nafion exhibits 2-5 nm hydrophilic ionic clusters surrounded by a matrix of the hydrophobic polymer backbone to create an interconnected channel-like structure. 21-23 The fixed, negatively-charged sulfonate groups selectively transport cations and water through the Nafion membrane dependent on electrostatic interactions and solvation energies. The anionic character of the sulfonate groups also diminishes anion transport significantly. 24, 25 In this study, Nafion is harnessed as an ion selective phase with the ability to create concentrated cation reservoirs relative to bulk solution concentrations. As demonstrated in a series of elegant studies by Marken and coworkers, this intriguing system can be utilized to create nanofluidic diodes with "on" and "off" states. 26-30

Here, we demonstrate modulation of ion transport properties across a silicon nitride (SiN_x) nanopore by the addition of Nafion. First, a comparison of the current-voltage response before and after the addition of the Nafion film was performed. Subsequently, a four-electrode SICM setup (**Figure 1**) was used to provide insight to variations in local ion concentration near the nanopore due to the induced ion concentration polarization. Application of different transmembrane potentials (V_{TM}) across the nanopore dictates the directionality of cation migration, and therefore, the location of the ion enrichment zone within the nanopore/Nafion/nanopipette environment. Current versus distance curves (i.e., approach curves) were acquired to probe local conductivity near the SiN_x nanopore.

Finite element method simulations (FEM) were performed to support experimental studies and rationalize ion concentration distributions of the nanopore, Nafion film, and nanopipette as a result of the applied V_{TM} .

Experimental

Materials. Potassium chloride (KCI, Sigma-Aldrich) was used as received. A dispersion of D2021 NafionTM (1100 EW, 20 wt%, alcohol-based, Fuel Cell Store) was used to prepare a 10 wt% solution of Nafion. All aqueous solutions were prepared with Milli-Q water (resistivity = 18.2 MΩ·cm at 25 °C, Thermo Scientific) and filtered with a 0.20 μm PVDF nylon syringe filter (MicroLiter). Single-window silicon nitride TEM grids were purchased from Norcada Inc. (NT025A).

Probe fabrication. Quartz capillaries (Q100-70-7.5, Sutter Instrument) were pulled with a CO₂-laser puller (P-2000, Sutter Instrument) to fabricate single barrel nanopipettes. A typical program used the following parameters: *Heat: 620, Velocity: 3, Filament: 40, Delay time: 180, Pull: 155*. Pipettes were characterized by scanning electron microscopy (SEM, FEI Quanta-FEG), with a typical inner radius of 25 - 30 nm and an outer radius of 45 - 50 nm (**Figure S1**).

Sample fabrication. An FEI Helios NanoLab 460F1 dual beam focused ion beam (FIB) was used to mill a nanopore through the 50 nm thick silicon nitride window with a 30 kV ion beam at a current of 7.7 pA. Nanopore size was characterized by SEM as shown in **Figure 2**. For the Nafion-coated SiN_x nanopore sample, Nafion solution (10 wt%) was drop cast onto the silicon nitride side of the TEM grid followed by spin coating at 3500 rpm for 30 s to form a Nafion film. The sample was placed in the oven for 1 h at 120 °C.³¹

Nafion film thickness was determined via a surface profiler (Bruker DektakXT Profiler) to be $1-1.3~\mu m$. Samples were mounted in a perfusion cell and hydrated in 0.1 M KCl overnight to allow for the Nafion film to equilibrate prior to measurement.

Current-voltage measurements. A two-electrode system was used to perform current-voltage (I-V) measurements with a picoammeter/voltage source (Keithley 6487, Keithley Instruments). A Ag/AgCl pellet was placed in the bottom chamber of solution which served as the working electrode and a second Ag/AgCl electrode was placed in the top chamber to serve as the reference electrode. The potential was stepped from -1 V to 1 V at 0.1 V/s.

SICM instrumentation. SICM measurements were performed with a custom-built SICM previously described elsewhere.³² The sample was mounted between two chambers of a perfusion cell with both chambers filled with 0.1 M KCI. The reference electrode (RE, Ag/AgCI) and counter electrode (CE, Pt) were placed in the top chamber and held at ground with a customized electrode-control module. The working electrode (WE, Ag/AgCI) was placed in the bottom chamber and biased to apply a transmembrane potential (V_{TM}) across the sample as shown in Figure 1. A function generator (33220A, Agilent Technologies) was used to apply the V_{TM} to the WE with respect to ground (RE and CE). A nanopipette filled with 0.1 M KCI, that contained a Ag/AgCI electrode served as the pipette electrode (PE). All data channels (XYZ piezo sensor voltages, ion current, and V_{TM}) were monitored in real time with an Axon Digidata 1440A (Molecular Devices) and Clampex 10.6 (Molecular Devices). Topography maps were collected to locate the nanopore within the SiN_x membrane (Figure S2). For approach curves, the pipette was intentionally not positioned directly above the center of the nanopore to prevent the

pipette from crashing into the membrane due to steep changes in ion concentration at the nanopore. The pipette's lateral (XY) position was held at a constant X-Y coordinate and approach curves were measured as V_{TM} was varied.

Finite element method (FEM) simulations. FEM simulations were carried out on an AMD EPYC 7403P 24-core processor by COMSOL Multiphysics (V6.1) with transport of diluted species and electrostatic modules to simultaneously solve for the electric potential and flux distribution. A two-dimensional axisymmetric model was used to represent the nanopipette at various positions away from the bare SiN_x nanopore and the Nafion-coated SiN_x nanopore. Geometry of the pipette and nanopore dimensions used in the model were determined by SEM. The Nafion film was modeled as a space charge density domain with different diffusion coefficient termed (D_{Nafion}) for potassium and chloride.^{25, 27} For more details of the FEM simulation see the Supporting Information file.

Results and Discussion

Current-Voltage Measurements

The simplest method to characterize ion transport properties through nanostructures is with current-voltage (I-V) measurements. The I-V response across the SiN_x nanopore is shown in **Figure 2a** alongside an electron micrograph of the corresponding nanopore, **Figure 2b**. The response displayed a linear trend that obeys Ohm's law with a resistance of approximately ~8 M Ω in 0.1 M KCI. The linear response of this pore is expected due to lack of electrochemical asymmetry and relatively large opening of the pore.³³⁻³⁶ Addition of Nafion to one side of the SiN_x membrane induced strong ion current rectification, as

shown in **Figure 2c**. The Nafion-coated SiN_x nanopore rectified current such that positive currents, with cations sourced from the Nafion side, were several times larger than negative currents, corresponding to cations sourced from the opposite side of the membrane. To quantify the degree of rectification, the ion current rectification ratio (ICRR) was calculated, where the current magnitude at each potential maximum (± 1V) was compared (ICRR = |I+v/I-v|). Thus, a value near unity indicates a linear I-V response. For negative rectification, the ICRR value ranges from one to infinity, whereas, for positive rectification the ICRR value ranges from one to zero. The ICRR value for the Nafion-coated SiN_x nanopore is 60.578 in comparison to 1.062 when no Nafion is present. The I-V responses of the Nafion-coated SiN_x nanopore differs from the response of a free-standing cation-exchange membrane, where the I-V curve has three distinct regions. ^{12, 37} Instead, the addition of Nafion has converted the SiN_x nanopore into an ionic diode, that displays an 'on' and 'off' state. ³⁸⁻⁴² These results are qualitatively in agreement with reported I-V measurements and voltammograms at the microscale. ^{26, 27, 29, 43}

The presence of ion current rectification indicates that concentrations of ions in the pore and at the pore entrances are voltage dependent. As mentioned above, when the positively biased electrode is placed on the side with Nafion, cations are sourced from the ion-exchange membrane. Note that Nafion's thickness (~1.2 μ m) is significantly larger than the thickness of the SiN_x membrane (50 nm), and the accepted space charge density for Nafion (1100 EW) is 1.63×10^8 C/m³,⁴⁴ thus the cation concentration in the Nafion exceeds the bulk concentration. Moreover, the cation migration from the bottom chamber toward the top chamber is not limited or diminished due to the dimensions of the nanopore. Furthermore, the bottom side of the Nafion film is in contact with the bulk

solution which can easily replenish the cation concentration within the film. We expect that positive V_{TM} will lead to enhancement of the concentration of cations in the pore and at the pore mouth, which in turn necessitates an increase of anion concentration as well to fulfill electroneutrality. These enhanced ion concentrations result in positive currents 8 times larger than currents for the silicon nitride pore without Nafion. On the other hand, with negatively biased electrode placed on the Nafion side, cations are sourced from the opposite opening (top reservoir) through the resistive pore to enter Nafion, while anions cannot be sourced from the Nafion film. As a result, a depletion zone is expected to form that limits the overall conductance. The nearly voltage-independent currents at negative voltages suggests that the depletion zone quickly spans a significant portion of the pore volume and determines the system's limiting conductance.

In **Figure 3**, three different sizes (100 nm, 150 nm, and 200 nm diameter, left to right, respectively) of Nafion-modified nanopores were imaged with a pipette bias of 200 mV and no applied V_{TM}. In this image, pores appear as raised features, possibly due to Nafion protruding through the membrane after spin coating. However, the influence of Nafion on surface charge and local ion concentrations complicates definitive image interpretation by SICM. Additionally, when a transmembrane potential was applied, local ion concentrations were altered to an extent that image collection was extremely difficult or impossible. Thus, to examine ion concentrations in detail, we utilized approach curves as described below.

Approach Curve Measurements to Bare Silicon Nitride Nanopore

Current-voltage curves recorded before and after the addition of Nafion suggest that the local ionic concentrations are strongly affected by the applied transmembrane potential,

 V_{TM} . To probe the extent of the modulation of local ionic concentrations, we recorded approach curves with SICM. First, we analyzed a SiN_x pores as prepared and second repeated the measurements on Nafion-coated SiN_x pores.

We began with SICM topographical mapping to locate the nanopore (**Figure S2**). The pipette position was subsequently moved $\sim 200-300$ nm from the center of the nanopore and held at a constant X-Y position. Approach curves (ion current as a function of z-position) were collected by measuring the pipette ion current as the pipette approached from the bulk electrolyte towards the SiN_x membrane at a rate of 13 nm/ms until the steady-state ion current decreased by the set threshold of 1.2%. **Figure 4** shows measurements for a SiN_x pore without Nafion, where the averaged approach curves were normalized by the steady state ion current, and Z-displacement denotes the distance the pipette retracted once the threshold ion current was achieved. Black traces are averaged approach curves measured when $V_{TM} = 0$, which displayed typical ion current-distance dependence governed by the resistance of the pipette and the distance-dependent access resistance.

Approach curves as well as the steady state current changed significantly once the V_{TM} was switched to positive or negative values (with the pipette potential held constant at 0.2 V (**Figure 4, top**)). With positive V_{TM} , the steady state current diminished and the approach curve exhibited a monotonic decrease as the pipette moved towards the surface. On the other hand, once the V_{TM} became negative, the steady state current increased and the approach current kept increasing, until the pipette reached the region where access resistance began to dominate and the current quickly decayed. We also considered the case when the pipette potential was -0.2 V (**Figure 4, bottom**), and again

applied positive and negative V_{TM} . In this case, the steady state current and approach curves exhibited an opposite dependence on the polarity of V_{TM} compared to the case with PE = 0.2 V. Namely, for positive V_{TM} (or negative V_{TM}) the ion current increased (or decreased) as the pipette moved closer to the surface.

All measurements shown in **Figure 4** can be explained by a circuit analysis for the experimental setup used in this study (**Figure S3** and **Table S1**). The recordings are in good agreement with the equivalent circuit model for a 4-electrode SICM setup separated by a porous membrane as previously reported.^{45, 46} Note that the access resistance acts as a voltage divider in all four cases shown in **Figure 4**. As such, when the potential at the WE electrode changes, with potential at PE held constant, the solution potential in the vicinity of the pore changes as well, influencing the ion current measured at the pipette. As an example, with $V_{TM} = 0.2 \text{ V}$, the pipette approaches the region with finite positive potential, such that the potential difference across the pipette becomes lower, which leads to lower pipette currents. With negative V_{TM} and PE = 0.2 V, the pipette approaches a region with small negative potential, which leads to a larger potential difference across the pipette, and higher currents. Experimental approach curves for the SiNx nanopore were substantiated by FEM simulations of approach curves to a SiNx nanopore under the application of $V_{TM} = 0.0 \text{ V}_{TM} = 0.2 \text{ V}$, and $V_{TM} = -0.2 \text{ V}$ (**Figure S5**).

Approach Curve Measurements to Nafion-coated Silicon Nitride Nanopore

Approach curves for a single SiN_x pore could be explained by the equivalent electric circuit where both the pipette and the pore are linear devices with constant resistance. Once

Nafion is introduced to the system, the SiN_x pore is changed into an ionic diode, whose resistance depends on voltage polarity and magnitude. Consequently, as discussed above we expected local ionic concentrations in the pore and in the regions next to pore openings to be modulated by V_{TM} , which we investigated by SICM.

The Nafion-coated SiN_x nanopore was characterized by approach curves recorded for four cases (Figure 5) with the same potentials for PE and V_{TM} used for the bare SiN_x pore, **Figure 4.** To begin, the analysis for positive V_{TM}, i.e., when the SiN_x/Nafion system is in its 'on' state with currents increase with voltage in a highly nonlinear manner. The I-V curve in Figure 2 suggests that ionic concentration in the pore and at the pore entrance are enhanced in voltage-dependent manner. Note that the concentrations of both cations and anions will be higher than in the bulk. Consequently, despite the positive pipette potential of PE = 0.2 V, the ion current through the pipette becomes strongly enhanced as the pipette approaches the region with high ionic conductivity (Figure 5, left). In addition, larger magnitudes of V_{TM} lead to a stronger enhancement of ionic concentrations, as observed by the increased magnitude of the current peak. Higher transmembrane potentials also significantly extended the region with enhanced concentrations. As an example, at $V_{TM} = 0.1 \text{ V}$, the strong increase of the pipette current started at Z-displacement of ~0.5 μ m, while at V_{TM} = 0.2 V, the current started to increase steeply at Z-displacement of $\sim 1.5 \mu m$.

Consider when PE = -0.2 V with positive V_{TM} , in this case, the Nafion-coated SiN_x nanopore is still in the 'on' state which produces enhanced ionic concentrations and enhanced current as the pipette approaches the Nafion-coated SiN_x nanopore from the bulk. Comparison of the SICM results for bare SiN_x and Nafion-coated SiN_x system

indicates that the observed trends in approach curves are independent of the pipette potential and are primarily governed by V_{TM} modulation of local ionic concentrations that the pipette senses. This conclusion is strengthened by the recordings with negative V_{TM} , which produced decreased steady state currents and approach curves for PE = -0.2 V and PE = 0.2 V (**Figure 5**, right). Negative V_{TM} corresponds to the 'off' state of the Nafion/SiN_x diode, which leads to decreased concentrations at the pore entrance and in the pore, and consequently lower pipette currents.

Finite Element Method (FEM) Simulations

In order to understand the extent of how the Nafion/SiN_x system can modulate ionic concentrations in the pore and at pore entrance, FEM simulations of ion concentrations and electric potential were performed. The simulation was simplified by alignment of the nanopipette and nanopore down their axis of symmetry, which allowed us to build a centrosymmetric model. More details on the numerical modeling can be found in the Supporting Information file.

Simulated approach curves for PE = 0.2 V are shown in **Figure 6a-c** and simulated approach curves for PE = -0.2 V are shown in **Figure S7**. These data are in good agreement with the experimental recordings shown in **Figure 5** such that the pipette current increased for positive V_{TM} . The chloride and potassium concentration distribution at $V_{TM} = 0.2$ V, when the pipette was positioned at $D_{PS} = 27$ nm, are plotted in **Figure 6d**. The gap between the tip of the pipette and the Nafion film indeed displays a higher concentration of both ions compared to the bulk solution, as suggested by the SICM

measurements. Additionally, ionic concentrations down the center axis of the nanopipette and nanopore are plotted, **Figure 6g**, at $V_{TM} = 0.2$ V, where the pipette tip is at z-coordinate of zero and the SiN_x nanopore thickness (50 nm) is indicated by the gray dashed lines. The ion concentration increases closer to the Nafion film, which is highly concentrated with potassium ions. Note that the whole pore volume and a large region in the top reservoir are filled with enhanced ionic concentrations of both types of ions. Consequently, simulated ion current increased as D_{PS} decreased as shown in **Figure 6a** due to the enhancement.

Figure 6e and **h** considers ionic distributions at $V_{TM} = 0$ V. The concentration of both ions is similar to the bulk concentration in the pore and at the pore entrances. Consequently, the system can be described by a typical approach curve explained by an equivalent electric circuit model. Finally, when $V_{TM} = -0.2$ (**Figure 6f** and **i**) the nanopore region displays a depletion zone with ionic concentrations below bulk values. Strikingly, these results suggest that the depletion of both ions occurs even at the Nafion-nanopore interface and propagates out toward the bulk solution when V_{TM} is biased negatively. As a result, the simulated ion current decreased as the pipette was stepped toward the nanopore due to depletion of both ions as shown in **Figure 6c**. The normalized ion current at $D_{PS} = 27$ nm was lower compared to **Figure 6a** and **b** due to the ion concentration being around 60 mM versus ~150 mM for **Figure 6a** and ~100 mM for **Figure 6b**.

Conclusion

Nafion coupled with a nanopore system allowed for controlled ion transport and amplification of ion current compared to a bare SiN_x nanopore. Current-voltage measurements across the Nafion-coated nanopore exhibited strong ion current enhancement at positive potentials compared to the bare SiN_x nanopore. Ion current rectification indicated that ion concentration polarization was occurring in Nafion/SiNx system that resulted in ionic diode behavior. SICM was successfully implemented to study local ion concentration as the nanopipette moved from the bulk solution toward the nanopore-Nafion interface. Approach curves confirmed that at positive V_{TM} both cations and anions were enhanced in nanopore and proximity due to the high flux of cations migrating from the Nafion film into the nanopore. Results demonstrated that control of the V_{TM} polarity and magnitude allowed for tuning the location and magnitude of ion enrichment and depletion in the Nafion/SiN_x nanopore system. By control of the applied V_{TM}, localized concentration gradients can be manipulated for chemical sensing at specific locations. In the future, the Nafion/SiN_x ionic diode can be coupled with additional nanofluidic circuitry for iontronics.

Acknowledgements

Electronic Instrument Services at Indiana University is acknowledged for designing and building the electronic devices. The National Science Foundation (CBET-220830) is acknowledged for support of this work. We thank AggieFab Nanofabrication Facility for access and use of instrumentation.

Reference

- 1. W. Shi, A. K. Friedman and L. A. Baker, *Analytical Chemistry*, 2017, **89**, 157-188.
- 2. K. Fu and P. W. Bohn, ACS Central Science, 2018, 4, 20-29.
- 3. G. Pérez-Mitta, M. E. Toimil-Molares, C. Trautmann, W. A. Marmisollé and O. Azzaroni, *Advanced Materials*, 2019, **31**, 1901483.
- M. Nazari, A. Davoodabadi, D. Huang, T. Luo and H. Ghasemi, ACS Nano, 2020, 14, 16348-16391.
- 5. Z. Zhang, L. Wen and L. Jiang, *Chemical Society Reviews*, 2018, **47**, 322-356.
- 6. K. Zhou, J. M. Perry and S. C. Jacobson, *Annual Review of Analytical Chemistry*, 2011, **4**, 321-341.
- 7. Z. Zhang, L. Wen and L. Jiang, *Nature Reviews Materials*, 2021, **6**, 622-639.
- 8. B. Berzina and R. K. Anand, *Analytica Chimica Acta*, 2020, **1128**, 149-173.
- 9. Z. Slouka, S. Senapati and H.-C. Chang, *Annual Review of Analytical Chemistry*, 2014, **7**, 317-335.
- 10. S. J. Kim, Y.-A. Song and J. Han, *Chemical Society Reviews*, 2010, **39**, 912-922.
- 11. T. A. Zangle, A. Mani and J. G. Santiago, *Chemical Society Reviews*, 2010, **39**, 1014-1035
- 12. J. J. Krol, M. Wessling and H. Strathmann, *Journal of Membrane Science*, 1999, **162**, 145-154.
- 13. S. J. Kim, Y.-C. Wang, J. H. Lee, H. Jang and J. Han, *Physical Review Letters*, 2007, **99**, 044501.
- 14. Q. Pu, J. Yun, H. Temkin and S. Liu, *Nano Letters*, 2004, **4**, 1099-1103.
- 15. F. C. Leinweber and U. Tallarek, *Langmuir*, 2004, **20**, 11637-11648.
- 16. I. Nischang, G. Chen and U. Tallarek, *Journal of Chromatography A*, 2006, **1109**, 32-50.
- 17. C. Zhu, K. Huang, N. P. Siepser and L. A. Baker, *Chemical Reviews*, 2021, **121**, 11726-11768.
- 18. N. Sa and L. A. Baker, *Journal of the American Chemical Society*, 2011, **133**, 10398-10401.
- 19. N. Sa, W.-J. Lan, W. Shi and L. A. Baker, ACS Nano, 2013, 7, 11272-11282.
- 20. C. Zhu, L. Zhou, M. Choi and L. A. Baker, *ChemElectroChem*, 2018, **5**, 2986-2990.
- 21. K. A. Mauritz and R. B. Moore, *Chemical Reviews*, 2004, **104**, 4535-4586.
- 22. K. Schmidt-Rohr and Q. Chen, Nature Materials, 2008, 7, 75-83.
- 23. A. Kusoglu and A. Z. Weber, *Chemical Reviews*, 2017, **117**, 987-1104.
- 24. W. H. Koh and H. P. Silverman, Journal of Membrane Science, 1983, 13, 279-290.
- 25. I. A. Stenina, P. Sistat, A. I. Rebrov, G. Pourcelly and A. B. Yaroslavtsev, *Desalination*, 2004, **170**, 49-57.
- 26. K. J. Aoki, L. Liu, F. Marken and J. Chen, *Electrochimica Acta*, 2020, **358**, 136839.
- 27. D. He, E. Madrid, B. D. B. Aaronson, L. Fan, J. Doughty, K. Mathwig, A. M. Bond, N. B. McKeown and F. Marken, *ACS Applied Materials & Interfaces*, 2017, **9**, 11272-11278.
- 28. Z. Li, T. Pang, J. Shen, P. J. Fletcher, K. Mathwig and F. Marken, *Micro and Nano Engineering*, 2022, **16**, 100157.
- 29. K. Mathwig, B. D. B. Aaronson and F. Marken, *ChemElectroChem*, 2018, **5**, 897-901.
- 30. B. R. Putra, E. Madrid, L. Tshwenya, O. A. Arotiba and F. Marken, *Desalination*, 2020, **480**, 114351.
- 31. B. Ilic, P. Neuzil, T. Stanczyk, D. Czaplewski and G. J. Maclay, *Electrochemical and Solid-State Letters*, 1999, **2**, 86.
- 32. L. Zhou, Y. Gong, J. Hou and L. A. Baker, *Analytical Chemistry*, 2017, **89**, 13603-13609.
- 33. M. L. Kovarik, K. Zhou and S. C. Jacobson, *The Journal of Physical Chemistry B*, 2009, **113**, 15960-15966.
- 34. Z. S. Siwy and S. Howorka, *Chemical Society Reviews*, 2010, **39**, 1115-1132.

- 35. Z. S. Siwy, Advanced Functional Materials, 2006, **16**, 735-746.
- 36. P. Ramírez, P. Y. Apel, J. Cervera and S. Mafé, Nanotechnology, 2008, 19, 315707.
- 37. I. Rubinstein and L. Shtilman, *Journal of the Chemical Society, Faraday Transactions 2: Molecular and Chemical Physics*, 1979, **75**, 231-246.
- 38. I. Vlassiouk and Z. S. Siwy, *Nano Letters*, 2007, **7**, 552-556.
- 39. I. Vlassiouk, S. Smirnov and Z. Siwy, ACS Nano, 2008, 2, 1589-1602.
- 40. L.-J. Cheng and L. J. Guo, *Chemical Society Reviews*, 2010, **39**, 923-938.
- 41. B. Lovrecek, A. Despic and J. Bockris, *The Journal of Physical Chemistry*, 1959, **63**, 750-751.
- 42. R. Karnik, C. Duan, K. Castelino, H. Daiguji and A. Majumdar, *Nano Letters*, 2007, **7**, 547-551.
- 43. L. Liu, K. J. Aoki and J. Chen, *Electrochem*, 2020, **1**, 400-409.
- 44. A. C. Barbati and B. J. Kirby, *Langmuir*, 2014, **30**, 1985-1993.
- 45. C.-C. Chen, Y. Zhou and L. A. Baker, *ACS Nano*, 2011, **5**, 8404-8411.
- 46. Y. Zhou, C.-C. Chen and L. A. Baker, *Analytical Chemistry*, 2012, **84**, 3003-3009.

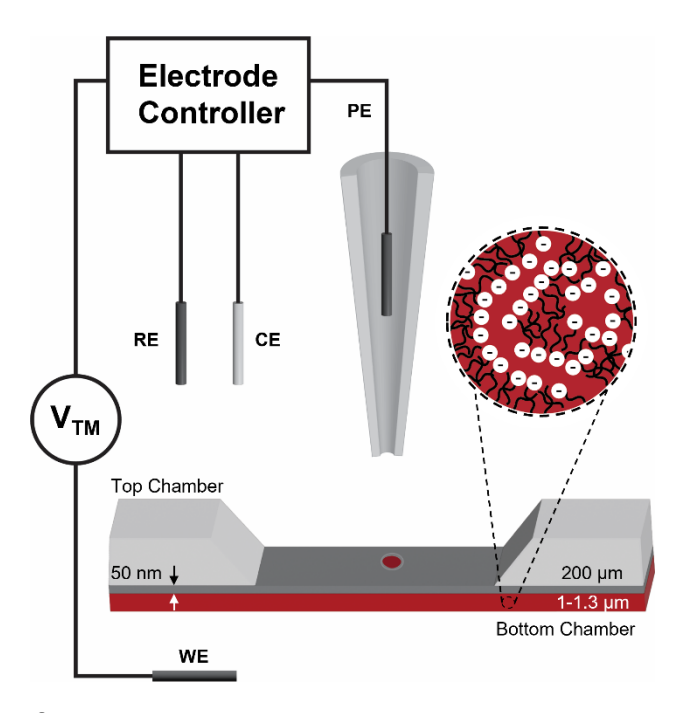


Figure 1. Schematic of the experimental setup where the transmembrane potential (V_{TM}) is applied at the working electrode (WE) across the Nafion film and through the nanopore. Inset: cartoon representation of the negative sulfonate groups within the Nafion film that allow selective cation transport.

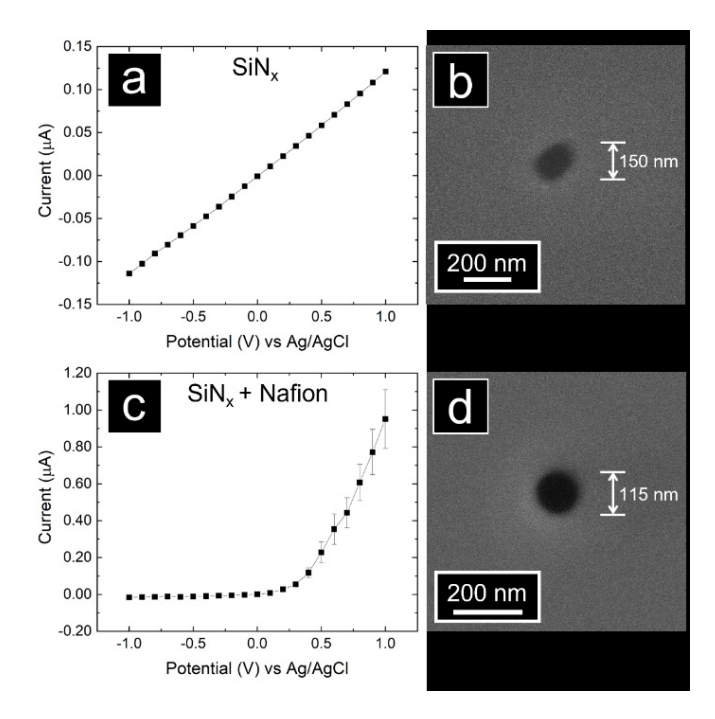


Figure 2. Current-voltage (I-V) response across a SiN_x nanopore (a) and a Nafion-coated SiN_x nanopore (Nafion thickness of ~1.2 µm) (b) in 0.1 M KCl at a step rate of 0.1 V/s (n=3). (b, d) Electron micrographs of the SiN_x (thickness of 50 nm) nanopores fabricated with a focused ion beam for the bare SiN_x nanopore sample (a) and for the Nafion-modified SiN_x nanopore sample (b).

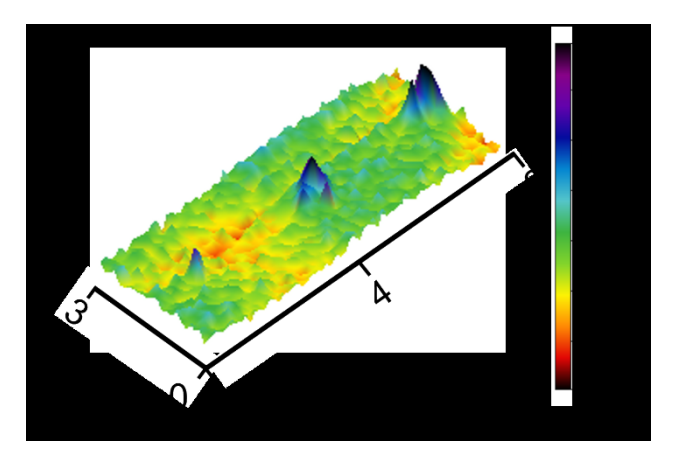


Figure 3. Three-dimensional topography image of Nafion-coated SiN_x nanopores with diameters of ~100 nm, 150 nm, and 200 nm in 0.1 M KCl. Imaged via SICM and collected at a pipette potential of 0.2 V and V_{TM} = 0 V with a current setpoint of 98.6% and resolution of 125 nm/pixel.

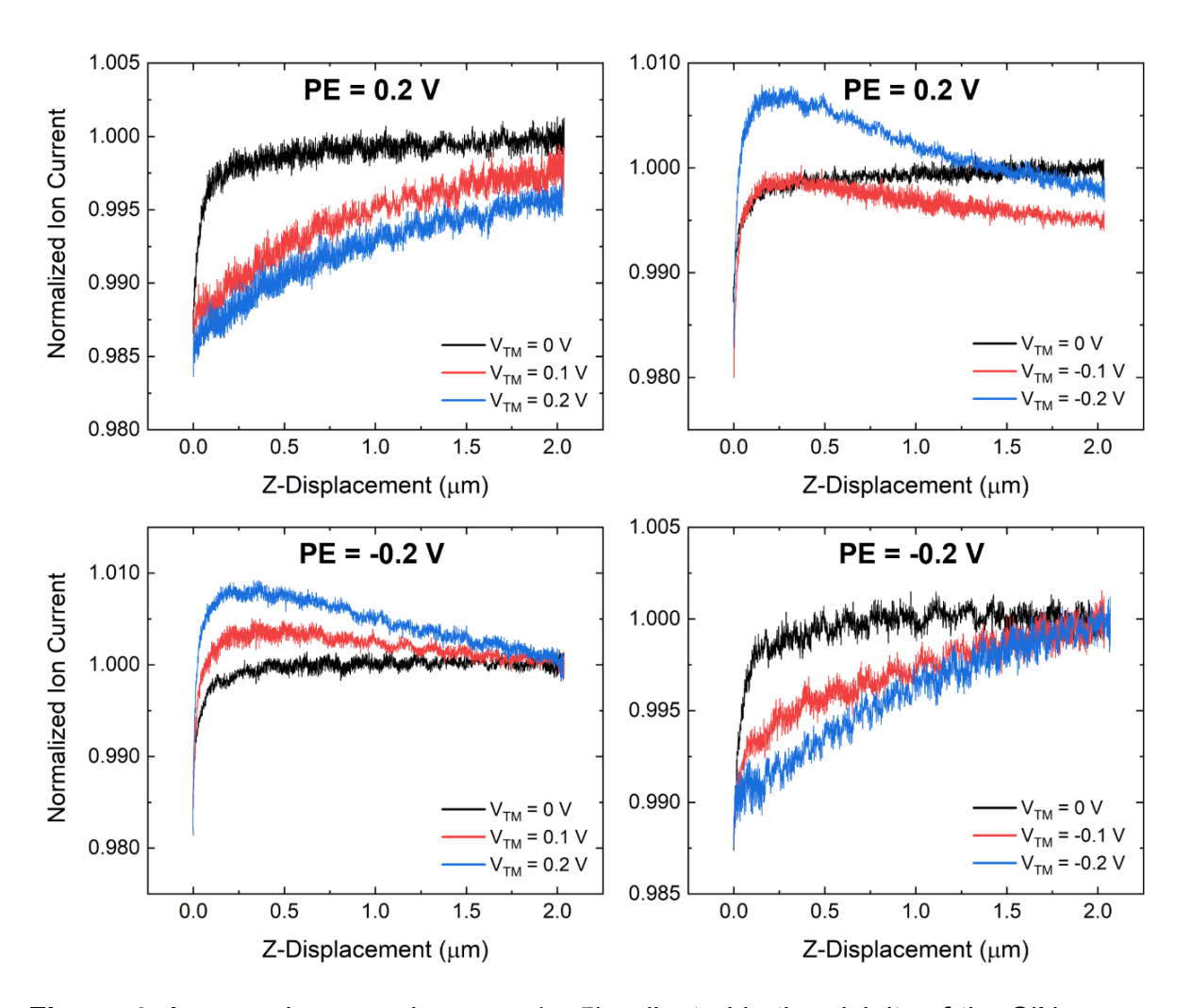


Figure 4. Averaged approach curves (n=5) collected in the vicinity of the SiN_x nanopore as the transmembrane potential (V_{TM}) is stepped positively (left) and negatively (right) at pipette potentials of PE = 0.2 V (top) and PE = -0.2 V (bottom) in 0.1 M KCl.

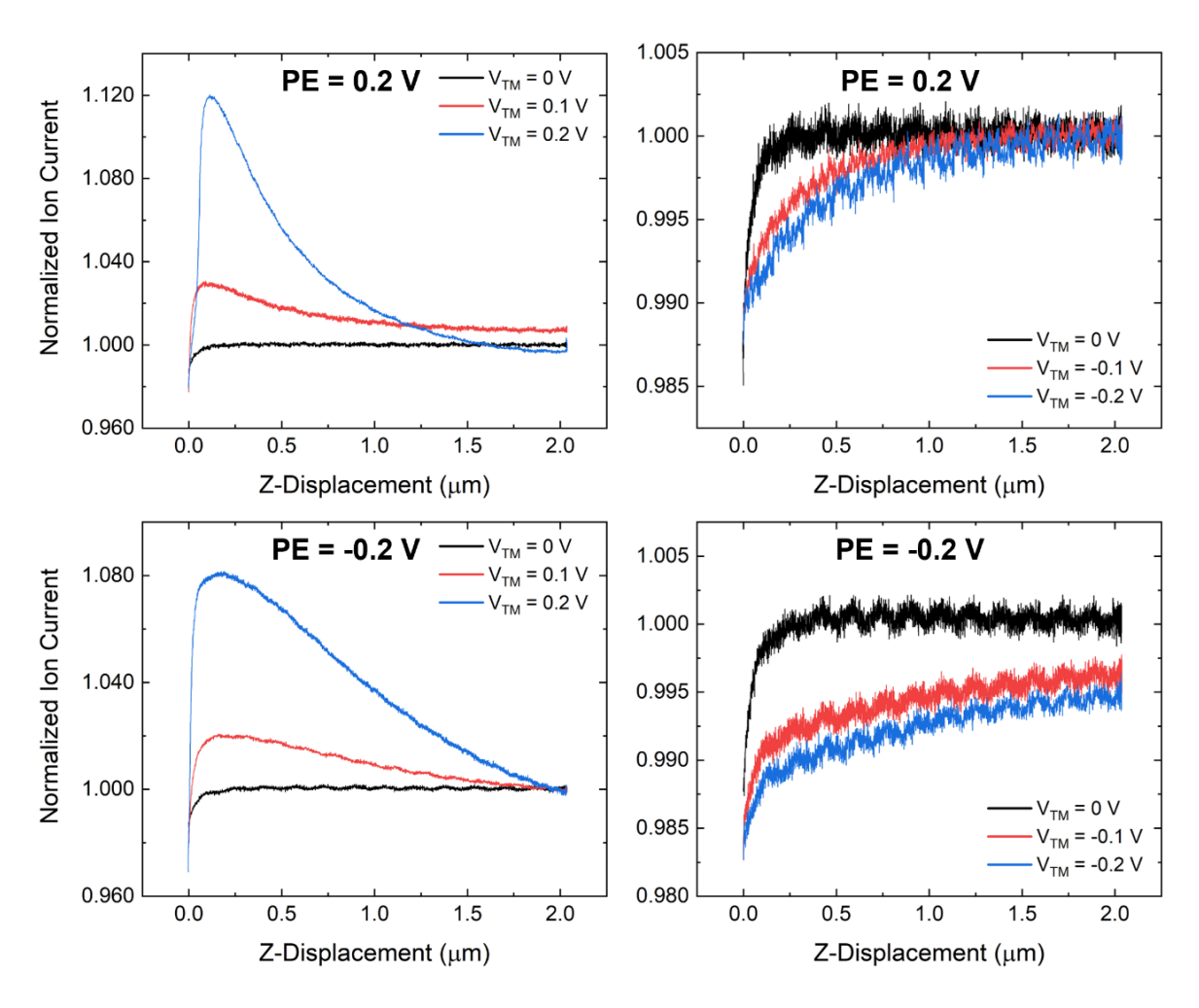


Figure 5. Averaged approach curves (n=5) measured in the vicinity of the Nafion-coated SiN_x nanopore as the transmembrane potential (V_{TM}) is stepped positively (left) and negatively (right) at pipette potentials of PE = 0.2 V (top) and PE = -0.2 V (bottom) in 0.1 M KCI.

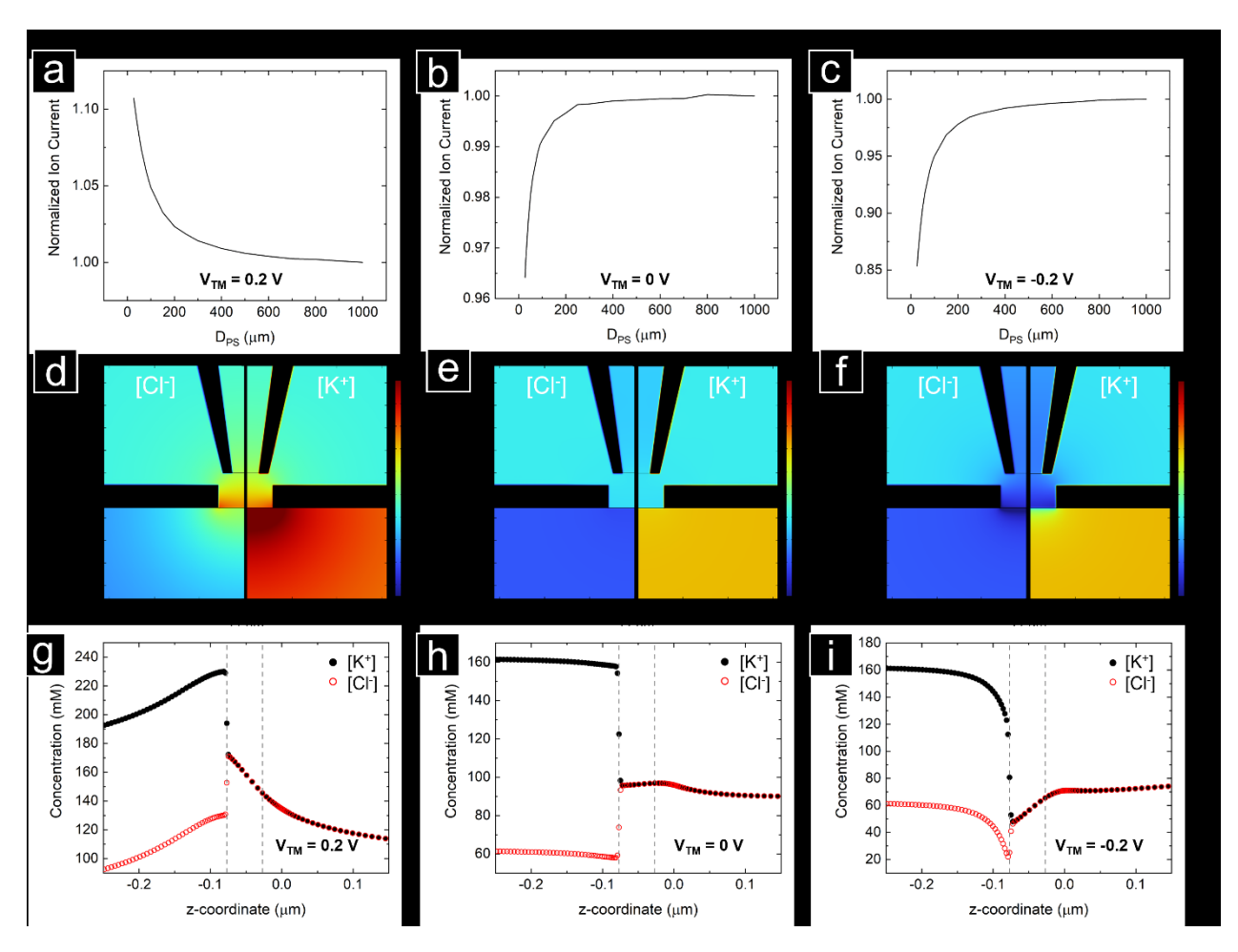


Figure 6. Simulated approach curves (PE = 0.2 V) towards the Nafion-coated SiN_x nanopore at V_{TM} = 0.2 V (a), 0 V (b), and -0.2 V (c). Corresponding ion concentration distribution at D_{PS} = 27 nm from the membrane (d-f) and line profile of the ion concentration down the axis of symmetry (g-i). Gray dashed lines indicate the length of the silicon nitride nanopore.